nature photonics

LETTERS

PUBLISHED ONLINE: 16 JUNE 2013 | DOI: 10.1038/NPHOTON.2013.131

Towards isolated attosecond pulses at megahertz repetition rates

Manuel Krebs[1]*, Steffen Hädrich[1,2], Stefan Demmler[1], Jan Rothhardt[1,2], Amelle Zaïr[3], Luke Chipperfield[4], Jens Limpert[1,2] and Andreas Tünnermann[1,2,5]

The strong-field process of high-harmonic generation is the foundation for generating isolated attosecond pulses[1], which are the fastest controllable events ever induced. This coherent extreme-ultraviolet radiation has become an indispensable tool for resolving ultrafast motion in atoms and molecules[2,3]. Despite numerous spectacular developments in the new field of attoscience[2–4], the low data-acquisition rates imposed by low-repetition-rate (maximum of 3 kHz) laser systems[5] hamper the advancement of these sophisticated experiments. Consequently, the availability of high-repetition-rate sources will overcome a major obstacle in this young field. Here, we present the first megahertz-level source of extreme-ultraviolet continua with evidence of isolated attosecond pulses using a fibre laser-pumped optical parametric amplifier[6] for high-harmonic generation at 0.6 MHz. This 200-fold increase in repetition rate will enable and promote a vast variety of new applications, such as attosecond-resolution coincidence and photoelectron spectroscopy[7], or even video-rate acquisition for spatially resolved pump–probe measurements.

It was realized early on that the process of high-harmonic generation (HHG) could give rise to subfemtosecond bursts of coherent extreme-ultraviolet (XUV) radiation[8–10]. This potential was demonstrated over a decade ago[1,11], and the process of HHG has since been used in a wide range of applications, including atomic and molecular physics[12,13], surface science[14] and imaging[15]. The emission of XUV radiation results from the interaction of an intense laser field with atoms or molecules. The strong field bends the Coulomb barrier, enabling a bound electronic wave packet to tunnel out of the barrier and move away from the parent ion. When the laser electrical field reverses, the wave packet is accelerated back to the parent ion and can recombine, emitting an XUV photon. This process occurs twice per laser cycle, resulting in the emission of an attosecond pulse train. For laser pulse durations of only a few cycles the emission of the highest energetic photons can be confined to a single event, leading to the generation of an isolated attosecond pulse (IAP)[9,16]. This technique, referred to as amplitude gating, is traditionally performed using post-compressed Ti:sapphire amplifier systems[17]. Alternative gating techniques have also been developed to circumvent the strict requirement on pulse duration[4,18]. However, all such schemes rely on a laser architecture limited in repetition rate due to thermo-optical constraints. Although sources for high-repetition-rate HHG and other strong-field processes emerged early[19–21], IAP generation has not exceeded a repetition rate of a few kilohertz[3,5]. This has severely limited, or hindered, a multitude of applications, in particular in terms of signal-to-noise ratio or statistics in the detection of photoelectrons or ionization fragments[3].

In recent years, optical parametric amplification has been regarded as a promising concept for advancing attosecond laser physics. Optical parametric amplifiers can offer an extremely large gain bandwidth, supporting few-cycle pulses with a great variety of wavelengths, and also have potential as high-repetition-rate sources of intense few-cycle pulses because of their outstanding thermo-optical properties.

In this work, we demonstrate a megahertz-level source of XUV continua showing evidence of isolated attosecond pulses, which overcomes the limitations of the current technology in attosecond science. A fibre laser-pumped two-stage optical parametric chirped pulse amplification (OPCPA) system[6] (Fig. 1a, see Methods) delivering carrier-envelope phase (CEP) stable 14 μJ pulses at a central wavelength of 918 nm (Fig. 1b), with a duration of 2.1 cycles (6.6 fs, Fig. 1c), was used to drive HHG in an argon gas jet (see Methods). After elimination of the fundamental radiation using a 200 nm aluminium filter, the resulting radiation was characterized spectrally and spatially using a flat-field grating spectrometer (see Methods). The CEP and chirp of the driving laser pulses were controlled by a pair of fused silica wedges. An adjustable iris can also be used to reduce the intensity in the interaction region to shift the cutoff photon energy below the L-absorption edge (73 eV, ref. 22) of aluminium.

In a first experiment, the OPCPA system was operated at 150 kHz. The HHG process was optimized in terms of gas pressure and jet position to achieve the highest XUV intensity in the cutoff, indicating phase-matched conversion to high photon energies. To obtain the best XUV continuum, a gas jet position behind the focus was chosen to select emissions arising due to short electron trajectories and to suppress those from long trajectories[23,24].

Figure 2a shows the behaviour of the HHG spectra for different relative CEP values. For certain values φ_0 of the CEP, the spectra are strongly modulated in the cutoff region, with a period of 2.71 eV (Fig. 2b), which is exactly twice the centre photon energy of the driving laser (1.36 eV). In the time domain, these modulations correspond to the interference of at least two XUV emission events separated by half of the laser optical cycle. This occurs when the electrical field of the generating few-cycle pulse is nearly sine shaped, leading to two laser field maxima separated by a half-cycle, with each generating an XUV pulse with a similar spectrum. The exact position of these harmonics in the spectrum strongly depends on the CEP of the incident pulses due to non-adiabatic effects in the rapidly changing electrical field of few-cycle pulses[25]. The latter effect also explains the shift in the harmonic position observed when scanning the CEP (Fig. 2a). In contrast, when the relative CEP is shifted to $\varphi_0 + \pi/2$, the interference in the cutoff

[1]Friedrich-Schiller-Universität Jena, Abbe Center of Photonics, Institute of Applied Physics, Albert-Einstein-Straße 15, 07745 Jena, Germany, [2]Helmholtz-Institute Jena, Fröbelstieg 3, 07743 Jena, Germany, [3]Blackett Laboratory, Imperial College London, Prince Consort Road, London SW7 2AZ, UK, [4]Max-Born Institute for Nonlinear Optics and Short Pulse Spectroscopy, Max-Born-Straße 2A, 12489 Berlin, Germany, [5]Fraunhofer Institute for Applied Optics and Precision Engineering, Albert-Einstein-Straße 7, 07745 Jena, Germany. *e-mail: manuel.krebs@uni-jena.de

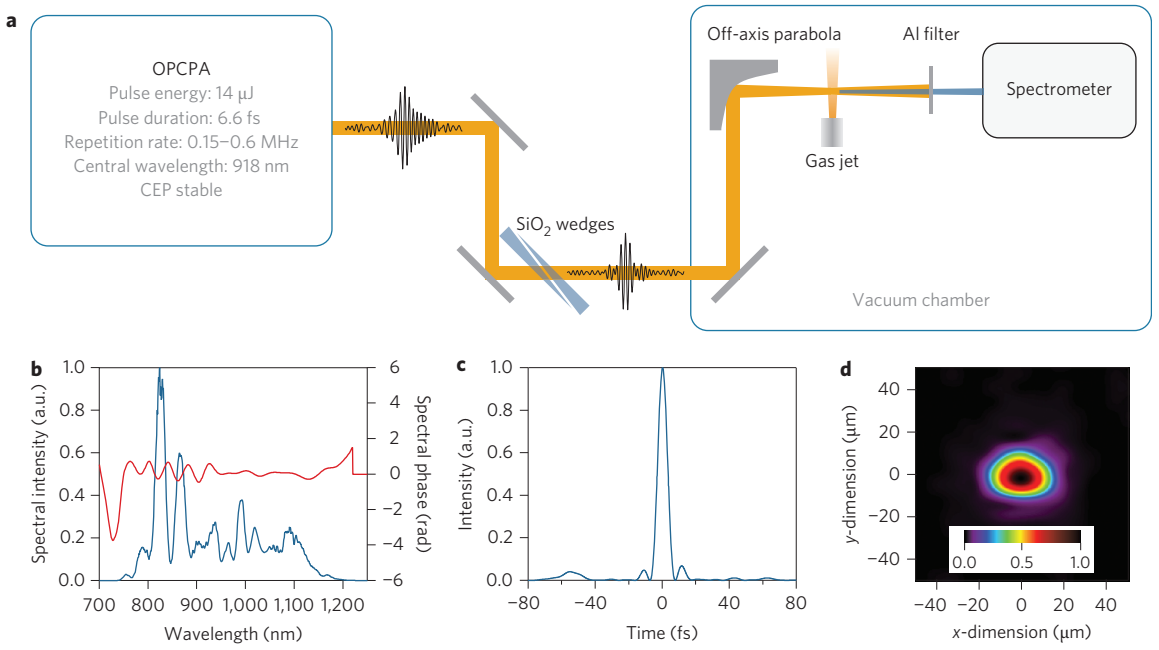

Figure 1 | Experimental set-up of the XUV source. a, An OPCPA system (see Methods) delivers CEP-stabilized laser pulses with a pulse energy of 14 μJ and a pulse duration of 6.6 fs at a central wavelength of 918 nm. The repetition rate can be varied between 150 kHz and 600 kHz. The pulses are steered to a vacuum chamber by silver mirrors and pass a pair of fused silica wedges under Brewster's angle for dispersion fine control and for variation of the CEP (see Methods). **b**, Spectral intensity (blue line) and phase (red line) of the few-cycle pulses generated by the OPCPA, as measured by SPIDER. **c**, Temporal envelope of the few-cycle pulses. **d**, A 1 mm fused silica substrate with a dispersion-optimized antireflection coating is used as the entrance window for the chamber. Focusing onto the argon gas jet is achieved by an $f = 75$ mm off-axis parabolic mirror, leading to a spot size of 35 μm × 30 μm. The resulting spectrum is recorded with a flat-field grating spectrometer (see Methods).

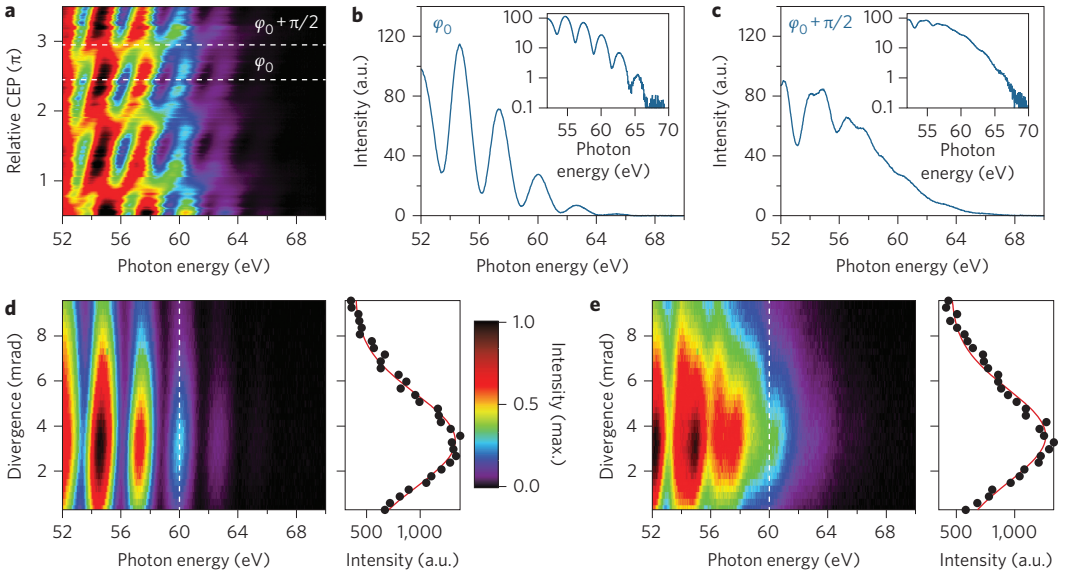

Figure 2 | HHG at 150 kHz repetition rate. a, Variation of the HHG spectrum in the cutoff region with respect to the CEP. For certain CEP values φ_0, there are strong spectral modulations, but these modulations disappear for the highest harmonics at $\varphi_0 + \pi/2$. The disappearance of the modulations indicates that there is only one strong emission event, that is, an isolated attosecond pulse. **b**,**c**, Corresponding lineouts for the relative CEP values, φ_0 and $\varphi_0 + \pi/2$, respectively. Insets: spectra on a logarithmic scale. **d**,**e**, Images taken with the CCD camera attached to the flat-field grating spectrometer (see Methods) for relative CEP values of φ_0 (**d**) and $\varphi_0 + \pi/2$ (**e**). The horizontal axis shows the spectrum and the vertical axis the divergence of the individual harmonics. The panels adjacent to each image show a spatial lineout (black dots) taken at a photon energy of 60 eV (indicated by the white dashed lines) together with a Gaussian fit (red lines).

region vanishes and a spectral continuum is formed (Fig. 2c). In this case, the laser electrical field is nearly cosine shaped, and only one half-cycle has enough intensity to generate the highest-energy photons. These photons form a single XUV pulse that shows no spectral interference. As expected by theory, the HHG spectra show a π-periodic behaviour[2]. The spatial structure of the highest harmonic orders is clean (Fig. 2d,e), indicating phase-matching between fundamental and short-trajectory generated harmonic

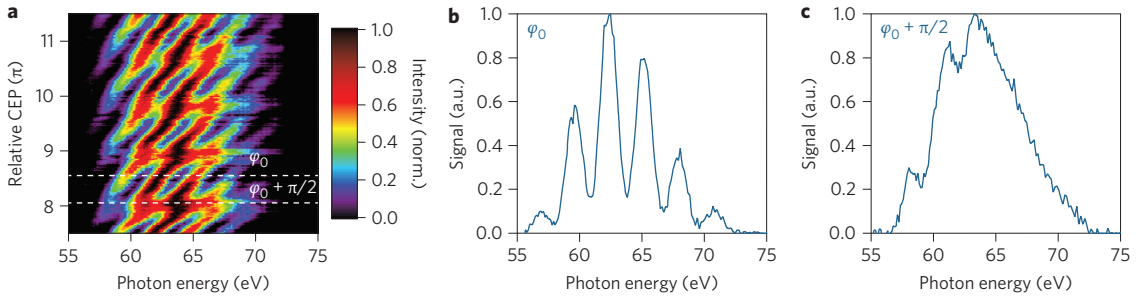

Figure 3 | Spectral selection of cutoff harmonics. An additional 200-nm-thick zirconium filter is placed before the spectrometer to spectrally select cutoff harmonics. The experiment was performed under slightly different conditions than in Fig. 2, leading to higher cutoff photon energies more suitable to the zirconium transmission. **a**, Scan showing the variation of the normalized harmonic spectrum with respect to the relative CEP. As already observed in Fig. 2a, there are certain relative CEP values that show strong modulations in the spectrum (φ_0), and shifting the CEP by $\pi/2$ results in a complete disappearance of the modulation and a continuous XUV spectrum corresponding to an isolated attosecond pulse. **b**, Lineout of the scan in **a** for a CEP of φ_0, with strong modulation (blue curve). **c**, Lineout of the scan in **a** for a CEP of $\varphi_0 + \pi/2$, with no modulation (blue curve).

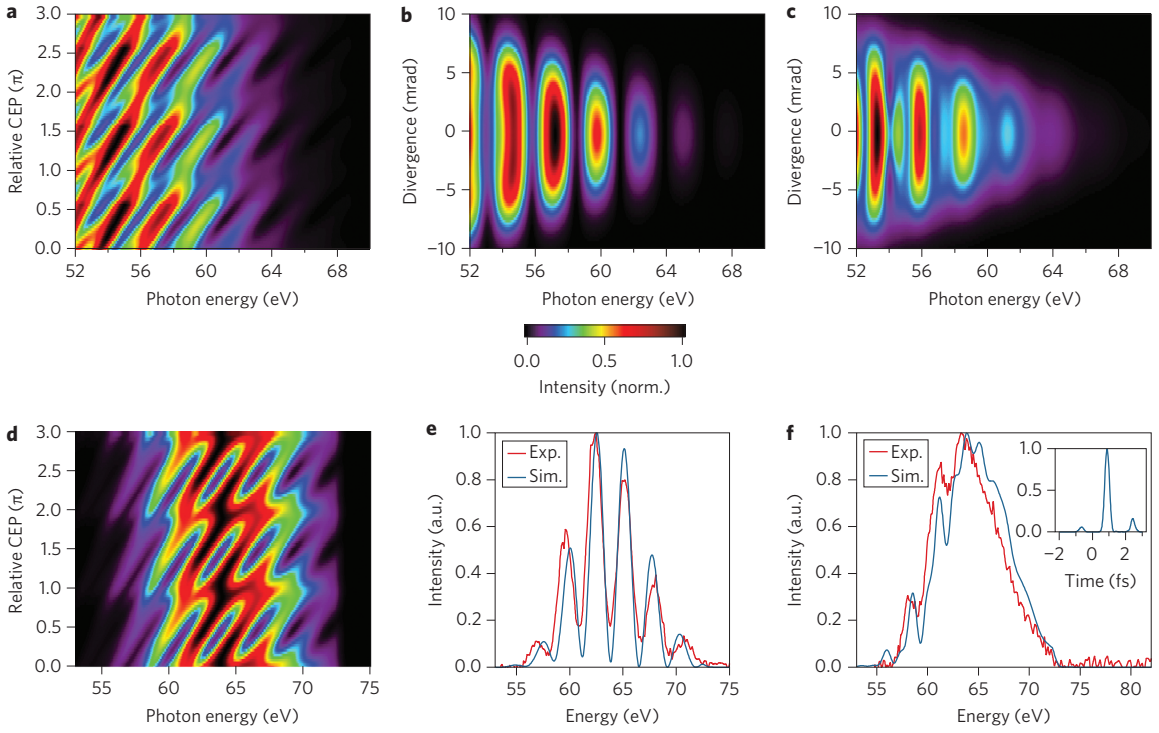

Figure 4 | Numerical simulation of the HHG process. The results of simulations of the HHG process are shown, the parameters of which have been adapted to the experimental conditions (see Methods). **a**, CEP dependence of the high harmonics, as observed in the experiments (Fig. 2a). The basic features of the experiment are reproduced by the simulation, such as the shift of the harmonic with respect to the CEP, the π-periodic behaviour and the continuum-like cutoff region for certain CEP values. **b**,**c**, Simulations also reproduce the spatial structure of the harmonics very well (Fig. 2d,e). **d**, CEP-dependent behaviour of the high-harmonic spectrum with an additional 200 nm zirconium filter to select the cutoff region. This completely agrees with the experimental data presented in Fig. 3a. **e**,**f**, Lineouts of the harmonic spectra show an excellent match between simulation (blue line) and experiment (red line). In conclusion, it is possible to reproduce our experimental findings with sufficient accuracy. This allows extraction of the basic temporal characteristics of the spectrally selected pulse, as shown in the inset of **f**. The simulations suggest that we have generated an isolated attosecond pulse (contrast ratio of 6.1:1) with a duration of 338 as.

radiation, which is particularly important for achieving well-defined and compressible spectral phase terms. Additionally, the generation conditions described here can be expected to lead to good spatial coherence[23].

Although the XUV emission is chirped, the XUV photons in the spectral continuum are generated within less than one quarter of the driving laser cycle, corresponding to an attosecond-timescale pulse duration. Selecting this part of the spectrum with a spectral filter suppresses the contributions from the adjacent laser cycles with lower intensity, and finally reveals an IAP[2]. In our experiment, an additional 200 nm zirconium filter was used to filter photon energies below 56 eV, and a similar behaviour of the harmonic spectra with respect to the CEP was observed (Fig. 3a–c). As a result of spectral filtering, the measurement shows the necessary clear signature for the formation of IAPs at a relative CEP of $\varphi_0 + \pi/2$ (Fig. 3c).

A simulation of the HHG process supports our experimental findings. It calculates the XUV field generated by an atomic gas

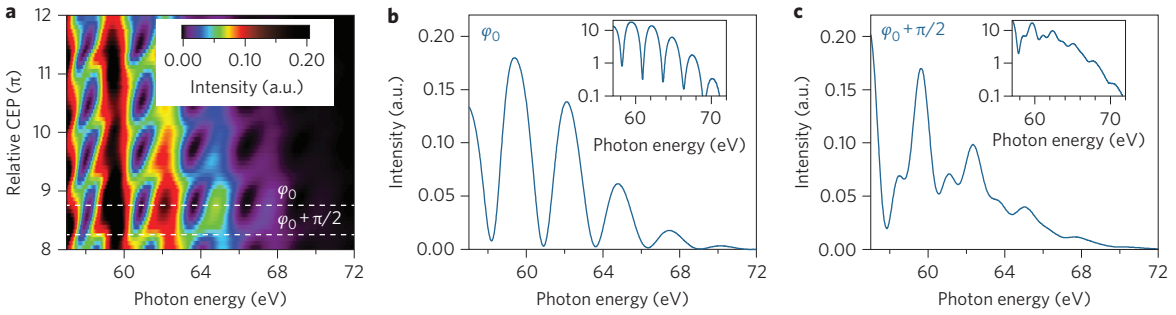

Figure 5 | HHG at 0.6 MHz repetition rate. In analogy to the results in Figs 2 and 3, the HHG process was investigated with the OPCPA system operated at 0.6 MHz (see Methods). **a,** Variation of the normalized HHG spectrum with respect to the CEP. For certain CEP values φ_0, there are strong spectral modulations, but these modulations disappear for the highest harmonics at $\varphi_0 + \pi/2$. The disappearance of the modulations indicates that there is only one strong emission event, that is, an IAP. **b**, Lineout of the scan in **a** for a CEP value of φ_0 with strong modulation. Inset: spectrum for φ_0 on a logarithmic scale. **c**, Lineout of the scan in **a** for a CEP value of $\varphi_0 + \pi/2$ with no modulation (blue curve). Inset: spectrum for $\varphi_0 + \pi/2$ on a logarithmic scale. The vanishing modulation indicates the generation of an isolated attosecond pulse.

when driven by an intense infrared laser field. This is achieved by solving the Maxwell wave equation coupled to the time-dependent Schrödinger equation (see Methods). The conditions in the simulation were adapted to those in our experiment. Comparing the simulation results (Fig. 4) with our measurements (Figs 2 and 3), we find that the simulation reproduces the experimental results both spectrally and spatially. As a consequence, although the spectral phase of the XUV radiation has not been measured directly, it seems valid to assume that the simulated phase matches the experiment with sufficient accuracy to characterize the generated pulses as IAPs. Furthermore, similar experimental observations of the high harmonic spectra[26] were later verified to produce IAPs[27], substantiating our statement. The temporal shape of the calculated pulse was characterized by a full-width at half-maximum (FWHM) duration of 338 as and a contrast ratio of 6.1:1 between the main pulse and the neighbouring pulses (Fig. 4f, inset).

So far, the generation of XUV continua has been demonstrated at 150 kHz, which already constitutes an enormous improvement over current low-kilohertz systems. The OPCPA system can be operated at even higher repetition rates while still preserving similar pulse parameters (see Methods). The resulting HHG spectra, scanned over different relative CEP values, are shown in Fig. 5a for the highest repetition rate of 0.6 MHz. In agreement with our earlier measurement, the π-periodicity and vanishing modulations for certain CEP values are clearly visible (Fig. 5b,c). The small variation in the spectral shape when compared to the lower repetition rate can be attributed to slightly different generation conditions (see Methods). Nevertheless, the scan shows a clear signature of isolated attosecond pulses in the cutoff region, and also demonstrates the scalability of our approach to megahertz-level repetition rates. An estimate of the photon flux (see Methods) contained in the continuum region (62–72 eV) yields 5.8×10^9 photons s^{-1}. As expected, this is roughly four times the flux obtained at a repetition rate of 150 kHz (1.3×10^9 photons s^{-1} in the 53–70 eV range).

In conclusion, we have demonstrated a megahertz-level repetition-rate source of XUV continua showing evidence of IAPs, which constitutes a 200-fold increase over conventional systems. Using our source, the detrimental space-charge effects of photoemission experiments such as photoemission spectroscopy[7], photoemission electron microscopy[28] or angle-resolved photoemission spectroscopy can be mitigated effectively because of the high photon flux, despite the moderate pulse energies. Hence, attosecond surface-science experiments, which have emerged as a key topic in attosecond physics, will benefit significantly. For the same reason, coincidence measurements with attosecond resolution, as well as reasonable acquisition times, become feasible. This paves the way for advanced attosecond-resolution experiments. Additionally, raising the repetition rate has the potential to dramatically improve most existing applications that are hindered by the low photon flux of conventional sources, by speeding up acquisition times and increasing the signal-to-noise ratio. Future development of fibre laser technology, which aims to achieve higher-pulse-energy OPCPA systems, will allow further enhancement of photon flux in the IAP generation process. Consequently, the enormous repetition rate enabled by fibre laser-pumped optical parametric amplification is a major milestone in the advancement of attosecond physics.

Methods

Two-cycle optical parametric amplification. Optical parametric amplification, which allows the amplification of exceptionally large bandwidths to high pulse energies, formed the basis of the driving laser system. Its principle design is described elsewhere[6]. Major modifications of this system were focused on achieving the best control of the electrical field of the pulses by proper spectral phase compensation and CEP stability. The seed pulses were delivered by a few-cycle Ti:sapphire oscillator (Femtolasers Rainbow), spectrally broadened, and temporally dispersed in an all-normal-dispersive photonic crystal fibre, sent through a spatial light modulator-based phase shaper (Biophotonic Solutions, 128 pixel, 600–1,230 nm) and subsequently amplified in two beta barium borate crystals with lengths of 2 mm and 1 mm, respectively. The pump laser, based on Yb-fibre laser technology, delivered frequency-doubled 100 μJ, 500 fs pulses at a wavelength of 515 nm, and variable repetition rate. It was optically synchronized to the master oscillator by means of soliton frequency shift in a photonic crystal fibre specially selected to have the lowest amplitude and timing jitter[6]. The two optical parametric amplification stages were optimized to generate a smooth output spectrum spanning from 750 nm to 1,250 nm, supporting a pulse duration of 6.4 fs. A chirped mirror compressor was used to compensate the second-order dispersion. Fourier-limited pulses were then achieved by measuring the residual spectral phase, including nonlinear contributions from the amplifiers[29], with the SPIDER pulse characterization technique[30] and compensation of the aforementioned phase utilizing the phase shaper. The compressed pulses were measured to be as short as 6.6 fs, which corresponds to only 2.1 optical cycles at a central wavelength of 918 nm. The compressed pulse energy was 14 μJ, resulting in a pulse peak power of 1.7 GW.

The system was operated at various repetition rates between 0.15 MHz and 0.6 MHz, with similar spectral and temporal characteristics of the output pulses. However, minor changes in beam divergence and diameter were observed at high repetition rates. Owing to the high nonlinearity of HHG, this slightly affects the generation conditions, as is obvious from Figs 2 and 4.

CEP stability. CEP stability is essential for the generation of IAPs as only this allows the control of the light fields required for this process[2]. In our laser system the carrier-envelope offset frequency of the seed oscillator was stabilized to one-quarter of its repetition rate. By selecting the repetition rate of the pump laser to be an integer fraction of this frequency, the seed pulses being amplified in the OPCPA had the same CEP. Although optical parametric amplification, in principle, preserves the CEP[31], attention has to be paid to the relative timing between pump and signal pulse. In our set-up it has to be stable within a few percent of the pump pulse duration to circumvent spectral distortions, which translate to CEP jitter via dispersion[32]. By isolating the beam path from mechanical vibrations and the housing of the laser system, and through active stabilization of the slow relative timing drifts, excellent

CEP stability was achieved. Integrating over 15 successive pulses (100 μs integration time), an r.m.s. jitter of 86 mrad was measured during 40 min of operation of the 150 kHz OPCPA system.

HHG. HHG was achieved by focusing the pulses from the OPCPA system into an argon gas jet formed by a 150-μm-diameter cylindrical nozzle. Applying an off-axis parabola as the focusing element avoided chromatic and spherical aberrations and allowed a focal spot size of 30 μm × 35 μm ($1/e^2$ intensity) to be achieved, as well as peak intensities up to $\sim 4 \times 10^{14}$ W cm^{-2} (Fig. 1d).

Characterization of the generated XUV radiation. A spectrometer (Ultrafast Innovations) with a gold-coated variable line spacing flat-field grating (nominal grating constant of 1,200 lines mm^{-1}) was used to image the high harmonic spectrum onto an XUV-sensitive charge-coupled device (CCD) camera. Imaging only took place in the spatial dimension perpendicular to the grating lines, so the beam propagated freely in the other dimension, enabling spectrally resolved one-dimensional beam profiles to be recorded. The spectrometer resolution was measured, using narrow line radiation, to be better than 100 meV FWHM around 60 eV. The CEP scans were measured by recording HHG spectra at a fixed rate while adjusting the wedge pair at a constant speed using a motorized translation stage. The appropriate relative CEP corresponding to each spectrum was calculated from the group and phase velocity of fused silica at the centre wavelength of 918 nm, as well as the total optical path length through the wedge pair. Based on a radiation power calibration of the CCD camera in the XUV range, the photon flux behind the gas jet was estimated by dividing the measured power at the CCD by the grating diffraction efficiency of 17% (value supplied by the manufacturer), the transmission coefficient of the aluminium filter[22] and the photon energy for each individual spectral component, then summing over the considered energy range.

Simulation. Propagation of the infrared field through the gas jet was simulated by solving the Maxwell wave equation after applying the slowly evolving wave approximation[33], including the time-dependent free-electron density as a source term[34]. Generation of the macroscopic XUV field occurs due to cooperative spontaneous emission from the ensemble of atoms within the gas jet. To simulate this, the single-atom dipole moment was calculated at each point on a spatial grid within the interaction region by solving the time-dependent Schrödinger equation after applying the strong field approximation[35]. The effect of the iris was implemented using a Hankel transform to propagate the laser pulse, which was initially given a Gaussian radial profile, from the beginning of the gas jet back to the iris, where it was radially clipped, and then forward to the gas jet again. A Hankel transform was again used to propagate the XUV field to the far field after it had exited from the gas jet. To mimic the experimental measurement, the spatial profiles shown in Fig. 4 were then calculated by taking an Abel transform of the XUV field.

The simulation parameters were adapted to best match the experimental data. To this end, the spectrum of the infrared laser field, on-axis at the focus with no iris, was set to the measured spectrum given in Fig. 1c, and the total pulse energy was set to the measured value of 14 μJ. For the gas jet, a parabolic density profile (peak density of 1×10^{19} cm^{-3} and an FWHM of 150 μm) was used. The focal geometry was then controlled by adjusting the diameter of the iris and the gas jet position.

The spectra plotted in Fig. 4a–c were generated using an iris aperture of 23.4 mrad with the gas jet positioned 1.27 mm after the focus. The XUV spectrum was then filtered by 200 nm of aluminium, taking account of dispersion[22]. The measurements recorded with the applied zirconium filter were simulated using a larger aperture of 27.3 mrad, a gas jet position 1.21 mm after the focus and two XUV filters (200 nm of aluminium and 200 nm of zirconium) (Fig. 4d–f).

Received 15 November 2012; accepted 24 April 2013; published online 16 June 2013

References

1. Hentschel, M. *et al.* Attosecond metrology. *Nature* **414,** 509–513 (2001).
2. Krausz, F. & Ivanov, M. Attosecond physics. *Rev. Mod. Phys.* **81,** 163–234 (2009).
3. Sansone, G., Calegari, F. & Nisoli, M. Attosecond technology and science. *IEEE J. Sel. Top. Quantum Electron.* **18,** 507–519 (2012).
4. Sansone, G., Poletto, L. & Nisoli, M. High-energy attosecond light sources. *Nature Photon.* **5,** 655–663 (2011).
5. Schultze, M. *et al.* Powerful 170-attosecond XUV pulses generated with few-cycle laser pulses and broadband multilayer optics. *New J. Phys.* **9,** 243 (2007).
6. Rothhardt, J., Demmler, S., Hädrich, S., Limpert, J. & Tünnermann, A. Octave-spanning OPCPA system delivering CEP-stable few-cycle pulses and 22 W of average power at 1 MHz repetition rate. *Opt. Express* **20,** 10870–10878 (2012).
7. Neppl, S. *et al.* Attosecond time-resolved photoemission from core and valence states of magnesium. *Phys. Rev. Lett.* **109,** 22–26 (2012).
8. Ferray, M. *et al.* Multiple-harmonic conversion of 1064 nm radiation in rare gases. *J. Phys. B* **21,** L31–L35 (1988).
9. Corkum, P., Burnett, N. & Ivanov, M. Y. Subfemtosecond pulses. *Opt. Lett.* **19,** 1870–1872 (1994).
10. Antoine, P., L'Huillier, A. & Lewenstein, M. Attosecond pulse trains using high-order harmonics. *Phys. Rev. Lett.* **77,** 1234–1237 (1996).
11. Paul, P. M. *et al.* Observation of a train of attosecond pulses from high harmonic generation. *Science* **292,** 1689–1692 (2001).
12. Baker, S. *et al.* Probing proton dynamics in molecules on an attosecond time scale. *Science* **312,** 424–427 (2006).
13. Smirnova, O. *et al.* High harmonic interferometry of multi-electron dynamics in molecules. *Nature* **460,** 972–977 (2009).
14. Miaja-Avila, L. *et al.* Direct measurement of core-level relaxation dynamics on a surface-adsorbate system. *Phys. Rev. Lett.* **101,** 46101 (2008).
15. Sandberg, R. L. *et al.* Lensless diffractive imaging using tabletop coherent high-harmonic soft-X-ray beams. *Phys. Rev. Lett.* **99,** 098103 (2007).
16. Christov, I. P., Murnane, M. M. & Kapteyn, H. C. High-harmonic generation of attosecond pulses in the 'single-cycle' regime. *Phys. Rev. Lett.* **78,** 1251–1254 (1997).
17. Baltuška, A. *et al.* Attosecond control of electronic processes by intense light fields. *Nature* **421,** 611–615 (2003).
18. Zair, A. *et al.* Time-resolved measurements of high order harmonics confined by polarization gating. *Appl. Phys. B* **78,** 869–872 (2004).
19. Lindner, F., Stremme, W., Schätzel, M. & Grasbon, F. High-order harmonic generation at a repetition rate of 100 kHz. *Phys. Rev. A* **68,** 013814 (2003).
20. Südmeyer, T. *et al.* Femtosecond laser oscillators for high-field science. *Nature Photon.* **2,** 599–604 (2008).
21. Gohle, C. *et al.* A frequency comb in the extreme ultraviolet. *Nature* **436,** 234–237 (2005).
22. Henke, B. L., Gullikson, E. M. & Davis, J. C. X-ray interactions: photoabsorption, scattering, transmission, and reflection at $E = 50$–$30{,}000$ eV, $Z = 1$–92. *Atom. Data Nucl. Data Tables* **54,** 181–342 (1993).
23. Salières, P., L'Huillier, A. & Lewenstein, M. Coherence control of high-order harmonics. *Phys. Rev. Lett.* **74,** 3776–3779 (1995).
24. Zaïr, A. *et al.* Quantum path interferences in high-order harmonic generation. *Phys. Rev. Lett.* **100,** 143902 (2008).
25. Nisoli, M. *et al.* Effects of carrier-envelope phase differences of few-optical-cycle light pulses in single-shot high-order-harmonic spectra. *Phys. Rev. Lett.* **91,** 213905 (2003).
26. Sola, I. J. *et al.* Controlling attosecond electron dynamics by phase-stabilized polarization gating. *Nature Phys.* **2,** 319–322 (2006).
27. Sansone, G., Benedetti, E., Vozzi, C., Stagira, S. & Nisoli, M. Attosecond metrology in the few-optical-cycle regime. *New J. Phys.* **10,** 025006 (2008).
28. Mikkelsen, A. *et al.* Photoemission electron microscopy using extreme ultraviolet attosecond pulse trains. *Rev. Sci. Instrum.* **80,** 123703 (2009).
29. Demmler, S. *et al.* Control of nonlinear spectral phase induced by ultra-broadband optical parametric amplification. *Opt. Lett.* **37,** 3933–3935 (2012).
30. Iaconis, C. & Walmsley, I. A. Spectral phase interferometry for direct electric-field reconstruction of ultrashort optical pulses. *Opt. Lett.* **23,** 792–794 (1998).
31. Baltuska, A. *et al.* Phase-controlled amplification of few-cycle laser pulses. *IEEE J. Sel. Top. Quantum Electron.* **9,** 972–989 (2003).
32. Hädrich, S. *et al.* Improving carrier-envelope phase stability in optical parametric chirped-pulse amplifiers by control of timing jitter. *Opt. Lett.* **37,** 4910–4912 (2012).
33. Brabec, T. & Krausz, F. Intense few-cycle laser fields: frontiers of nonlinear optics. *Rev. Mod. Phys.* **72,** 545–591 (2000).
34. Gaarde, M. B., Tate, J. L. & Schafer, K. J. Macroscopic aspects of attosecond pulse generation. *J. Phys. B* **41,** 132001 (2008).
35. Lewenstein, M. *et al.* Theory of high-harmonic generation by low-frequency laser fields. *Phys. Rev. A* **49,** 2117–2132 (1994).

Acknowledgements

This work was supported by the German Federal Ministry of Education and Research (BMBF), the European Research Council under the European Union's Seventh Framework Programme (FP7/2007-2013)/ERC grant agreement no. 240460, UK-EPSRC project EP/J002348/1 and UK Royal Society project IE121529. The authors thank E. Cormier for providing initial simulations and for fruitful discussions. L.C. thanks the Imperial College High Performance Computing Service for the use of their facilities.

Author contributions

J.L. conceived the initial idea. The experiments were planned, designed and performed by M.K., S.D., S.H. and J.R. with support from A.Z., L.C. and J.L. The experimental data were analysed by M.K. and S.H, and L.C. and A.Z. contributed the simulations and supported the interpretation of the results. J.L. and A.T. supervised the project and acquired funding. All authors contributed to the manuscript.

Additional information

Reprints and permissions information is available online at www.nature.com/reprints. Correspondence and requests for materials should be addressed to M.K.

Competing financial interests

The authors declare no competing financial interests.